

Particle Spectroscopy of Supersymmetric $SO(10)$ with Non-Universal Gaugino Masses

Nobuchika Okada ^{a,*}, Shabbar Raza ^{b,†} and Qaisar Shafi ^b

^a *Department of Physics and Astronomy, University of Alabama, Tuscaloosa, AL 35487, USA*

^b *Bartol Research Institute, Department of Physics and Astronomy, University of Delaware, Newark, DE 19716, USA*

We examine the low scale particle spectroscopy of an $SO(10)$ (or equivalently $SU(5)$) inspired supersymmetric model with non-universal gaugino masses. The model assumes minimal supergravity and contains the same number of fundamental parameters as the constrained minimal supersymmetric model (CMSSM.) Realistic solutions compatible with dark matter and other applicable experimental constraints are shown to exist for both positive and negative signs of the MSSM parameter μ . We present several benchmark points which will be tested at the LHC and by the ongoing direct and indirect dark matter detection experiments.

PACS numbers: 12.60.Jv, 12.10.Dm, 14.80.Ly

I. INTRODUCTION

The constrained minimal supersymmetric model (CMSSM), also referred to as mSUGRA, is based on the standard model gauge symmetry $SU(3) \times SU(2) \times U(1)$ and has the fewest number of fundamental parameters arising from the supersymmetric extension of the SM. Supersymmetry breaking in the CMSSM originates in some unspecified ‘hidden’ sector, which is then transmitted through gravity to our ‘visible’ sector. The lightest neutralino (LSP) in the CMSSM is stable and a leading dark matter candidate particle. Intense searches including direct, indirect and at the LHC, are currently underway to find the LSP. A flurry of recent papers by the ATLAS [1] and CMS [2] experiments at the LHC are beginning to constrain the CMSSM parameter space, which translates into new lower bounds on a variety of sparticle masses including the gluino and the squarks of the first two families.

The apparent unification at $M_G \sim 3 \times 10^{16}$ GeV of the CMSSM gauge couplings strongly suggests the presence of an underlying grand unified theory (GUT) such as $SU(5)$ or $SO(10)$. Since the three MSSM gauge multiplets reside in a single unified gauge multiplet of $SU(5)$ or $SO(10)$, it would seem quite natural that the various MSSM gauginos all acquire the same universal mass $M_{1/2}$ at M_G . However, the universal gaugino mass assumption is, in fact, not a general consequence of gravity mediated SUSY breaking. In the gravity mediation scenario, the gaugino masses are given by non-zero F -term of the gauge kinetic function which, generally, is in one of the irreducible representations of a symmetric product of two adjoint representations and hence, not necessarily a singlet. Therefore, if such a non-singlet develops a non-zero F -term, the MSSM gaugino masses can be expected to be non-universal. Interestingly, if we assume that a single non-zero F -term dominates the gauge kinetic function, the ratios between the MSSM gaugino masses are completely determined by group theory, depending only on the way the MSSM gauge multiplets are embedded in the symmetric product of two adjoint representations of the GUT gauge group. This means that the number of free parameters in a setup with non-universal gaugino masses (NUGM) remains the same as in the CMSSM, at least in the gauge sector.

In the MSSM, the lightest neutralino, if it is the LSP, is a primary candidate for the dark matter particle. Since the neutralino is an admixture of gauginos and Higgsinos, its mass and interaction with other (s)particles are determined by the masses of bino, wino and Higgsinos. Thus, a boundary condition involving non-universal gaugino masses can dramatically alter the phenomenology of neutralino dark matter from the CMSSM case [3]. In addition, the neutralino LSP plays a key role in the SUSY search at high energy colliders, and composition and mass of the neutralino being different from the CMSSM case has impact on SUSY searches at the Tevatron [4] and at the Large Hadron Collider (LHC) [5].

In this paper, we investigate the TeV scale particle spectroscopy of SUSY $SO(10)$ and $SU(5)$ inspired model with non-universal gaugino masses. Taking a variety of phenomenological constraints into account, in particular, the relic density of neutralino dark matter, we identify the allowed regions of the input SSB parameters for various $\tan \beta$ values. We consider both signs of the MSSM μ -parameter. For the allowed parameter region, we calculate the spin-independent (SI) and spin-dependent (SD) cross sections for neutralino elastic scattering off a nucleon, and compare our results with the current and proposed future bounds from direct and indirect dark matter search experiments. We also present several benchmark points from the allowed region and show the sparticle mass spectra, which can be tested at the LHC. The mass spectra are compared with those from the CMSSM with suitably fixed parameter sets.

*Electronic address: okadan@ua.edu.

†Electronic address: shabbar@udel.edu. On study leave from: Department of Physics, FUUAST, Islamabad, Pakistan.

II. NON-UNIVERSAL GAUGINO MASSES FROM $SO(10)$ AND $SU(5)$

We first review how the non-universal gaugino masses arise in the $SO(10)$ GUT. In gravity mediation, we introduce a higher dimensional operator between the gauge field strength superfield \mathcal{W}^a and a hidden sector chiral superfield Φ_{ab} ,

$$\mathcal{L} = \int d^2\theta \frac{\Phi_{ab}}{M_P} \mathcal{W}^a \mathcal{W}^b, \quad (1)$$

where $a, b = 1, 2, \dots, 45$ are the group indices for $SO(10)$, and $M_P = 2.4 \times 10^{18}$ GeV is the reduced Planck mass. In this paper, we consider only a single hidden sector field Φ_{ab} whose non-zero F -term breaks SUSY and generates the gaugino masses:

$$\mathcal{L} = \int d^2\theta \frac{\Phi_{ab}}{M_P} \mathcal{W}^a \mathcal{W}^b \supset \frac{F_{\Phi_{ab}}}{M_P} \lambda^a \lambda^b. \quad (2)$$

In $SO(10)$, a possible representation of the hidden sector field is given by one of the irreducible representations contained in the symmetric product of two adjoint 45-dimensional representations:

$$(45 \otimes 45)_{\text{sym}} = \mathbf{1} \oplus \mathbf{54} \oplus \mathbf{210} \oplus \mathbf{770}. \quad (3)$$

If the hidden sector field is not the singlet, non-universal masses for the MSSM gauginos are generated. However, the ratio between the MSSM gaugino masses is determined by the embedding of the SM gauge groups within each irreducible representation [6, 7].

Among the three possibilities in Eq.(3), we investigate Φ_{ab} in the $\mathbf{54}$ representation in this paper. In fact, this is the most reasonable case from the theoretical point of view. We are considering SUSY $SO(10)$ as a more fundamental theory within which the MSSM is embedded. We may expect that the $SO(10)$ model is further unified into a more fundamental theory including gravity, most likely some string theory at the Planck scale. Note that this picture constrains the field representations introduced in the model, since large representations carry a large β -function, and this can cause the $SO(10)$ gauge coupling to blow up below the Planck scale. Indeed, the introduction of an irreducible representation larger than 126 is excluded by this argument [8]. With the $\mathbf{54}$ -plet of hidden sector field, the ratios of the non-universal gaugino masses is found to be [7]

$$M_1 : M_2 : M_3 = -\frac{1}{2} : -\frac{3}{2} : 1 \quad (4)$$

The above discussion is readily extended to $SU(5)$, and the gluino mass ratios turn out to be the same as in Eq.(4) for a hidden sector field in the 24-dimensional adjoint representation [7]. Thus, our analysis in this paper applies both to $SO(10)$ and $SU(5)$ models. However, note that in the $SU(5)$ GUT, the matter multiplets of each family are not completely unified in a single representation and in general, the masses of sfermions in $\mathbf{5}^*$ and $\mathbf{10}$ representations can be non-universal. This non-universality of sfermion masses can serve as a probe to discriminate the underlying GUT gauge groups [9].

In the following, we identify the parameter region which is consistent with a variety of phenomenological constraints. Since the ratio between the non-universal gaugino masses is fixed as in Eq. (4), the number of free parameters remains the same as in the CMSSM. We use the notation $M_3 = M_{1/2}$, so that $M_1 = -\frac{1}{2}M_{1/2}$ and $M_2 = -\frac{3}{2}M_{1/2}$. The fundamental parameters of the $SO(10)/SU(5)$ model that we consider are as follows:

$$m_0, M_{1/2}, A_0, \tan \beta, \text{sign}(\mu). \quad (5)$$

III. PHENOMENOLOGICAL CONSTRAINTS AND SCANNING PROCEDURE

We employ the ISAJET 7.80 package [10] to perform random scans over the parameter space listed in Eq. (5). In this package, the weak scale values of gauge and third generation Yukawa couplings are evolved to M_{GUT} via the MSSM renormalization group equations (RGEs) in the \overline{DR} regularization scheme. We do not strictly enforce the unification condition $g_3 = g_1 = g_2$ at M_{GUT} , since a few percent deviation from unification can be assigned to unknown GUT-scale threshold corrections [11]. At M_{GUT} , the boundary conditions given in Eq. (5) are imposed and all the SSB parameters, along with the gauge and Yukawa couplings, are evolved back to the weak scale M_Z . The impact of the neutrino Dirac Yukawa coupling in the running of the RGEs is significant only for relatively large values (~ 2 or so) [12]. In the $SO(10)$ GUT we expect the largest Dirac coupling to be comparable to the top Yukawa coupling (~ 0.5 at M_{GUT}) and thus we safely neglect effects of the neutrino Dirac Yukawa coupling in our analysis.

In the evaluation of Yukawa couplings the SUSY threshold corrections [13] are taken into account at the common scale $M_{\text{SUSY}} = \sqrt{m_{\tilde{t}_L} m_{\tilde{t}_R}}$. The entire parameter set is iteratively run between M_Z and M_{GUT} using the full 2-loop RGEs until a

stable solution is obtained. To better account for leading-log corrections, one-loop step-beta functions are adopted for gauge and Yukawa couplings, and the SSB parameters m_i are extracted from RGEs at multiple scales $m_i = m_i(m_i)$. The RGE-improved 1-loop effective potential is minimized at an optimized scale M_{SUSY} , which effectively accounts for the leading 2-loop corrections. Full 1-loop radiative corrections are incorporated for all sparticle masses.

The requirement of radiative electroweak symmetry breaking (REWSB) [14] puts an important theoretical constraint on the parameter space. Another important constraint comes from limits on the cosmological abundance of stable charged particles [15]. This excludes regions in the parameter space where charged SUSY particles, such as $\tilde{\tau}_1$ or \tilde{t}_1 , become the LSP. We accept only those solutions for which one of the neutralinos is the LSP and saturates the dark matter relic abundance bound observed by the Wilkinson Microwave Anisotropy Probe (WMAP).

We perform random scans for the following parameter range:

$$\begin{aligned} 0 &\leq m_0 \leq 5 \text{ TeV} \\ 0 &\leq M_{1/2} \leq 2 \text{ TeV} \\ \tan \beta &= 10, 30, 50 \\ A_0 &= 0, 1, -1, 5, -5 \text{ TeV} \\ \mu &< 0, \mu > 0 \end{aligned} \tag{6}$$

with $m_t = 173.1 \text{ GeV}$ [16]. The results are not too sensitive to one or two sigma variation in the value of m_t . We use $m_b(m_Z) = 2.83 \text{ GeV}$ which is hard-coded into ISAJET.

In scanning the parameter space, we employ the Metropolis-Hastings algorithm as described in [17]. All of the collected data points satisfy the requirement of REWSB, with the neutralino in each case being the LSP. Furthermore, all of these points satisfy the constraint $\Omega_{\text{CDM}} h^2 \leq 10$. This is done so as to collect more points with a WMAP compatible value of cold dark matter (CDM) relic abundance. For the Metropolis-Hastings algorithm, we only use the value of $\Omega_{\text{CDM}} h^2$ to bias our search. Our purpose in using the Metropolis-Hastings algorithm is to be able to search around regions of acceptable $\Omega_{\text{CDM}} h^2$ more fully. After collecting the data, we impose the mass bounds on all the particles [15] and use the IsaTools package [18] to implement the following phenomenological constraints:

$$\begin{aligned} m_h \text{ (lightest Higgs mass)} &\geq 114.4 \text{ GeV} & [19] \\ BR(B_s \rightarrow \mu^+ \mu^-) &< 5.8 \times 10^{-8} & [20] \\ 2.85 \times 10^{-4} \leq BR(b \rightarrow s\gamma) &\leq 4.24 \times 10^{-4} \text{ (} 2\sigma \text{)} & [21] \\ 0.53 \leq \frac{BR(B_u \rightarrow \tau\nu_\tau)_{\text{MSSM}}}{BR(B_u \rightarrow \tau\nu_\tau)_{\text{SM}}} &\leq 2.03 \text{ (} 2\sigma \text{)} & [22] \\ \Omega_{\text{CDM}} h^2 &= 0.111_{-0.037}^{+0.028} \text{ (} 5\sigma \text{)} & [23] \\ 3.4 \times 10^{-10} \leq \Delta(g-2)_\mu/2 &\leq 55.6 \times 10^{-10} \text{ (} 3\sigma \text{)} & [24] \end{aligned}$$

We apply the experimental constraints successively on the data that we acquire from ISAJET.

IV. RESULTS

Figure 1 shows the results in the $(M_{1/2}, m_0)$ plane for $\tan \beta = 10$, $A_0 = 0$ and $\text{sign}(\mu) = \pm$. Gray points are consistent with successful REWSB and the requirement of neutralino LSP. Blue points satisfy the WMAP bounds on neutralino dark matter abundance, particle mass bounds, as well as constraints from $BR(B_s \rightarrow \mu^+ \mu^-)$, $BR(b \rightarrow s\gamma)$ and $BR(B_u \rightarrow \tau\nu_\tau)$. In Figure 1, the small boxes show benchmark points for each of which the particle mass spectra are listed in Tables I and II. We have chosen these benchmark points from regions in Figure 2 and 3, which can be explored by future dark matter search experiments (see below).

A variety of experiments are underway to directly detect dark matter particles through their elastic scatterings off nuclei. The most stringent limits on the (spin-independent) elastic scattering cross section have been reported by the recent CDMS-II and XENON100 experiments. In Figure 2 (the color coding is the same as in Figure 1) we show the results for the spin-independent elastic scattering cross section along with the current upper bounds by the CDMS-II [25] (solid black line) and XENON100 [26] (solid red line) experiments, as well as the future reach of the SuperCDMS(SNOLAB) [27] (dotted black line) and XENON1T [28] (dotted red line). In the $(\sigma_{\text{SI}}, m_{\tilde{\chi}_1^0})$ plane, there are dips in the resultant cross sections. Two of them around $m_{\tilde{\chi}_1^0} \sim 45 \text{ GeV}$ and $m_{\tilde{\chi}_1^0} \sim 57 \text{ GeV}$ correspond to Z- and Higgs resonances, respectively. Around these parameter regions, the neutralino annihilation cross sections are enhanced by the resonances and as a result, the correct relic abundance can be achieved with relatively small coupling constants. Thus, the corresponding spin-independent cross sections are reduced due to the small coupling constants. Another dip around $m_{\tilde{\chi}_1^0} \sim 200 \text{ GeV}$ in Figure 2 (a) corresponds to a cancellation between effective couplings of neutralino with up-quark and down-quark in Higgs exchange processes. As has been reported in [29], this cancellation occurs when the relative signs between $M_{1,2}$ and μ are opposite. Recall that in our convention, $M_3 > 0$ and

$M_{1,2} < 0$, so that this cancellation occurs for $\mu > 0$. The small boxes show the benchmark points corresponding to those listed in Tables I and II. These benchmark points have been chosen with the criterion that they should lie between the present experimental limits and future reaches. In the region from which the benchmark points are chosen, the neutralino LSP has sizable Higgsino components which, in turn, enhance the spin-independent neutralino-nucleon cross sections. All of the benchmark points can be tested by XENON1T, while SuperCDMS can explore some of them.

Neutralino dark matters in the galactic halo may become gravitationally trapped in the Sun and accumulate in its center, where they can annihilate each other and produce high energy neutrinos. Since neutrinos can escape and reach the Earth, the neutralino annihilations can be indirectly detected by observing an excess of such high energy neutrinos from the Sun. The most stringent limits on the neutrino flux from the Sun have been reported by Super-Kamiokande [30] and IceCube [31] experiments, which provide the upper limit on the spin-dependent elastic scattering cross section of neutralino dark matter off a nucleon. The spin-dependent scattering cross sections along with the current upper bounds and future reach are depicted in Figure 3. In this figure too, the color coding is the same as in Figure 1. In the $(\sigma_{SD}, m_{\tilde{\chi}_1^0})$ plane we show the results for the spin-dependent elastic scattering cross section along with the current bounds from Super-Kamiokande (black line) and IceCube (dotted black line) experiments, together with the future reach of IceCube DeepCore experiment (dotted red line). The small boxes show the approximate locations of benchmark points corresponding to Tables I and II. For these points, the sizable Higgsino components of the neutralino LSP enhances the scattering cross section. All benchmark points except for point 1 are testable by the future IceCube DeepCore experiment. Although the benchmark point 1 has a neutralino mass below the energy threshold of the IceCube DeepCore experiment, such a light neutralino can provide characteristic signatures in collider experiments.

Plots analogous to Figures 1-3 for varying values of $\tan\beta$ are shown in Figures 4-9 and the particle mass spectra of the corresponding benchmark points are listed in Tables III-VI. The figures for $\mu < 0$ show green points which belong to the subset of blue points and satisfy all constraints including $\Delta(g-2)_\mu/2$, where the deviation of the muon anomalous magnetic dipole moment from the SM prediction can be explained by sparticle loop contributions. Since the sparticle contributions to $\Delta(g-2)_\mu/2$ are dominated by loop diagrams with chargino and are proportional to $\mu M_2 \tan\beta / \tilde{m}_{SUSY}^4$, where \tilde{m}_{SUSY} is the sparticle mass in the loop, the relative sign of μ and M_2 should be positive ($\mu < 0$ in our convention) in order to obtain $\Delta(g-2)_\mu/2 > 0$. If the sparticles running in the loop diagrams are heavy, a relatively large $\tan\beta$ is necessary to satisfy the constraint from $\Delta(g-2)_\mu/2$. There is no green point in Figure 1 because $\tan\beta = 10$ is too small to be compatible with the $\Delta(g-2)_\mu/2$ constraint. We also list benchmark points (5 and 6 in Tables III-VI) with relatively large neutralino mass, some of which can/cannot be tested by the future IceCube DeepCore experiment.

For $|A_0| \leq \mathcal{O}(1 \text{ TeV})$, the results remain almost the same as those with $A_0 = 0$, and we therefore do not show all plots. The results for special cases with a large A_0 or a large $\tan\beta$ are depicted in Figure 10. The upper panel shows the results in the $(M_{1/2}, m_0)$ plane for $A_0 = -5 \text{ TeV}$, $\tan\beta = 10$ and $\mu < 0$. An almost identical plot is also obtained for the opposite sign of $\mu > 0$. There are two interesting regions. One is the usual stau co-annihilation region for $M_{1/2} \gtrsim 1 \text{ TeV}$, the other one is the region for $M_{1/2} \lesssim 1 \text{ TeV}$ where the mass difference between the neutralino LSP and lighter stop is small, and the desired relic abundance of neutralino dark matter is achieved through stop-neutralino co-annihilations. This stop-neutralino co-annihilation region only appears for a big negative A_0 . The lower panel corresponds to the results for a relatively large $\tan\beta (= 53)$ in the $(m_H, m_{\tilde{\chi}_1^0})$ plane. The allowed region appears for $2m_{\tilde{\chi}_1^0} \simeq m_H$ by the enhancement of neutralino annihilation cross sections via heavy Higgs boson exchange processes in the s -channel. For the chosen benchmark points, the mass spectra are listed in Table VII.

Finally, we choose several benchmark points from the allowed regions for different values of A_0 , $\tan\beta$ and $\text{sign}(\mu)$ and compare the mass spectra in our NUGM model with those from the CMSSM. In Table VIII, we present four benchmark points from the stau-neutralino co-annihilation region to compare the mass spectra. For the same values of A_0 , $\tan\beta$ and $\text{sign}(\mu)$, we tune m_0 and $M_{1/2}$ in the CMSSM in order to obtain the same masses for neutralino LSP and the lighter stau as those found in NUGM model. The resultant masses for the other particles are all larger than those in the CMSSM. In Table IX, we tune m_0 and $M_{1/2}$ in the CMSSM so as to give the same masses for gluino and right-handed down squarks as in the NUGM model. We can see, in this case, large mass differences in the neutralino and chargino mass spectra, while the sfermion mass spectra are similar. In particular, the mass of the neutralino LSP is relatively small as a result of the non-universal boundary conditions for the gaugino masses. The results in these Tables show that the mass spectra in our NUGM model are quite distinct from those in the CMSSM.

V. CONCLUSIONS

We have investigated the low scale particle spectroscopy arising from supersymmetric SO(10) and SU(5) models with non-universal gaugino masses. This non-universality generally arises from the F -term of some non-singlet hidden sector field in the gauge kinetic function in the gravity mediated supersymmetry breaking. Depending on the embedding of the MSSM gauge group, the ratio of the MSSM gaugino masses is determined by group theory. Among several possibilities, we have considered an F -term from a single 54-plet hidden sector field. This is a unique possibility if we require the SO(10) gauge coupling to stay within the perturbative regime up to the Planck scale. With the group theoretically fixed ratios of the gaugino masses, we

set the fundamental parameters of the model in the same way as the CMSSM, namely, m_0 , $M_{1/2}$, A_0 , $\tan\beta$ and $\text{sign}(\mu)$ with the identification $M_3 = M_{1/2}$. Taking a variety of phenomenological constraints into account, we have identified the allowed parameter regions. We have also calculated the spin-independent and dependent cross sections of neutralino elastic scattering off a nucleon and compared the results with the reach of future direct and indirect detection experiments. We have identified the benchmark points of the model which are consistent with the phenomenological constraints and which predict neutralino elastic scattering cross sections accessible at the future dark matter detection experiments. The particle mass spectra of the benchmark points can be well-distinguished at the LHC from the mass spectra in the CMSSM.

Note Added: t - b - τ Yukawa unification in this class of models with $\mu < 0$ has recently been investigated in [32].

Acknowledgments

We thank Ilia Gogoladze and Rizwan Khalid for useful comments and discussion. This work is supported in part by the DOE Grants, No. DE-FG02-10ER41714 (N.O.) and No. DE-FG02-91ER40626 (Q.S. and S.R.) and by Bartol Research Institute (S.R.). N.O. would like to thank the Particle Theory Group of the University of Delaware for hospitality during his visit.

-
- [1] G. Aad *et al.* [Atlas Collaboration], [arXiv:1102.2357](https://arxiv.org/abs/1102.2357) [hep-ex]; J. B. G. da Costa *et al.* [Atlas Collaboration], [arXiv:1102.5290](https://arxiv.org/abs/1102.5290) [hep-ex].
 - [2] V. Khachatryan *et al.* [CMS Collaboration], Phys. Lett. B **698**, 196 (2011) [[arXiv:1101.1628](https://arxiv.org/abs/1101.1628)] [hep-ex].
 - [3] A. Corsetti and P. Nath, Phys. Rev. D **64**, 125010 (2001); S. F. King, J. P. Roberts and D. P. Roy, JHEP **0710**, 106 (2007); K. Huitu and J. Laamanen, Phys. Rev. D **79**, 085009 (2009); U. Chattopadhyay, D. Das and D. P. Roy, Phys. Rev. D **79**, 095013 (2009); M. Holmes and B. D. Nelson, Phys. Rev. D **81**, 055002 (2010).
 - [4] G. Anderson, H. Baer, C. h. Chen and X. Tata, Phys. Rev. D **61**, 095005 (2000).
 - [5] S. Bhattacharya, A. Datta and B. Mukhopadhyaya, JHEP **0710**, 080 (2007); K. Huitu, J. Laamanen, P. N. Pandita and S. Roy, Phys. Rev. D **72**, 055013 (2005); K. Huitu, R. Kinnunen, J. Laamanen, S. Lehti, S. Roy and T. Salminen, Eur. Phys. J. C **58**, 591 (2008); S. Bhattacharya and J. Chakraborty, Phys. Rev. D **81**, 015007 (2010).
 - [6] N. Chamoun, C. S. Huang, C. Liu and X. H. Wu, Nucl. Phys. B **624** (2002) 81 [[arXiv:hep-ph/0110332](https://arxiv.org/abs/hep-ph/0110332)].
 - [7] S. P. Martin, Phys. Rev. D **79**, 095019 (2009) [[arXiv:0903.3568](https://arxiv.org/abs/hep-ph/0903.3568)] [hep-ph].
 - [8] D. Chang, T. Fukuyama, Y. Y. Keum, T. Kikuchi and N. Okada, Phys. Rev. D **71**, 095002 (2005).
 - [9] I. Gogoladze, R. Khalid, N. Okada and Q. Shafi, Phys. Rev. D **79**, 095022 (2009); N. Okada and H. M. Tran, Phys. Rev. D **83**, 053001 (2011).
 - [10] H. Baer, F. E. Paige, S. D. Protopopescu and X. Tata, [arXiv:hep-ph/0001086](https://arxiv.org/abs/hep-ph/0001086).
 - [11] J. Hisano, H. Murayama, and T. Yanagida, Nucl. Phys. **B402** (1993) 46. Y. Yamada, Z. Phys. **C60** (1993) 83; J. L. Chkareuli and I. G. Gogoladze, Phys. Rev. D **58**, 055011 (1998).
 - [12] For recent discussions and additional references see V. Barger, D. Marfatia and A. Mustafayev, Phys. Lett. B **665**, 242 (2008); M. E. Gomez, S. Lola, P. Naranjo and J. Rodriguez-Quintero, [arXiv:0901.4013](https://arxiv.org/abs/0901.4013) [hep-ph].
 - [13] D. M. Pierce, J. A. Bagger, K. T. Matchev, and R.-j. Zhang, Nucl. Phys. **B491** (1997) 3.
 - [14] L. E. Ibanez and G. G. Ross, Phys. Lett. **B110** (1982) 215; K. Inoue, A. Kakuto, H. Komatsu and S. Takeshita, Prog. Theor. Phys. **68**, 927 (1982) [Erratum-ibid. **70**, 330 (1983)]; L. E. Ibanez, Phys. Lett. **B118** (1982) 73; J. R. Ellis, D. V. Nanopoulos, and K. Tamvakis, Phys. Lett. **B121** (1983) 123; L. Alvarez-Gaume, J. Polchinski, and M. B. Wise, Nucl. Phys. **B221** (1983) 495.
 - [15] K. Nakamura *et al.* [Particle Data Group], J. Phys. G **37**, 075021 (2010).
 - [16] [Tevatron Electroweak Working Group and CDF Collaboration and D0 Collab], [arXiv:0903.2503](https://arxiv.org/abs/0903.2503) [hep-ex].
 - [17] G. Belanger, F. Boudjema, A. Pukhov and R. K. Singh, JHEP **0911**, 026 (2009); H. Baer, S. Kraml, S. Sekmen and H. Summy, JHEP **0803**, 056 (2008).
 - [18] H. Baer, C. Balazs, and A. Belyaev, JHEP **03** (2002) 042; H. Baer, C. Balazs, J. Ferrandis, and X. Tata Phys. Rev. **D64** (2001) 035004.
 - [19] S. Schael *et al.* Eur. Phys. J. C **47**, 547 (2006).
 - [20] T. Aaltonen *et al.* [CDF Collaboration], Phys. Rev. Lett. **100**, 101802 (2008).
 - [21] E. Barberio *et al.* [Heavy Flavor Averaging Group (HFAG) Collaboration], [arXiv:0704.3575](https://arxiv.org/abs/0704.3575) [hep-ex].
 - [22] D. Eriksson, F. Mahmoudi and O. Stal, JHEP **0811** (2008) 035.
 - [23] E. Komatsu *et al.* [WMAP Collaboration], Astrophys. J. Suppl. **180**, 330 (2009).
 - [24] G. W. Bennett *et al.* [Muon G-2 Collaboration], Phys. Rev. D **73**, 072003 (2006).
 - [25] Z. Ahmed *et al.* [The CDMS-II Collaboration], [arXiv:0912.3592](https://arxiv.org/abs/0912.3592) [astro-ph.CO].
 - [26] E. Aprile *et al.* [XENON100 Collaboration], [arXiv:1104.2549](https://arxiv.org/abs/1104.2549) [astro-ph.CO].
 - [27] T. Bruch and f. t. C. Collaboration, [arXiv:1001.3037](https://arxiv.org/abs/1001.3037) [astro-ph.IM].
 - [28] The XENON Dark Matter Project http://xenon.astro.columbia.edu/XENON100_Experiment/

- [29] J. R. Ellis, A. Ferstl, K. A. Olive, Phys. Lett. **B481**, 304-314 (2000). [[hep-ph/0001005](#)].
- [30] S. Desai *et al.* [Super-Kamiokande Collaboration], Phys. Rev. D **70**, 083523 (2004) [Erratum-ibid. D **70**, 109901 (2004)].
- [31] R. Abbasi *et al.* [ICECUBE Collaboration], Phys. Rev. Lett. **102**, 201302 (2009).
- [32] I. Gogoladze, Q. Shafi and C. S. Un, to appear.

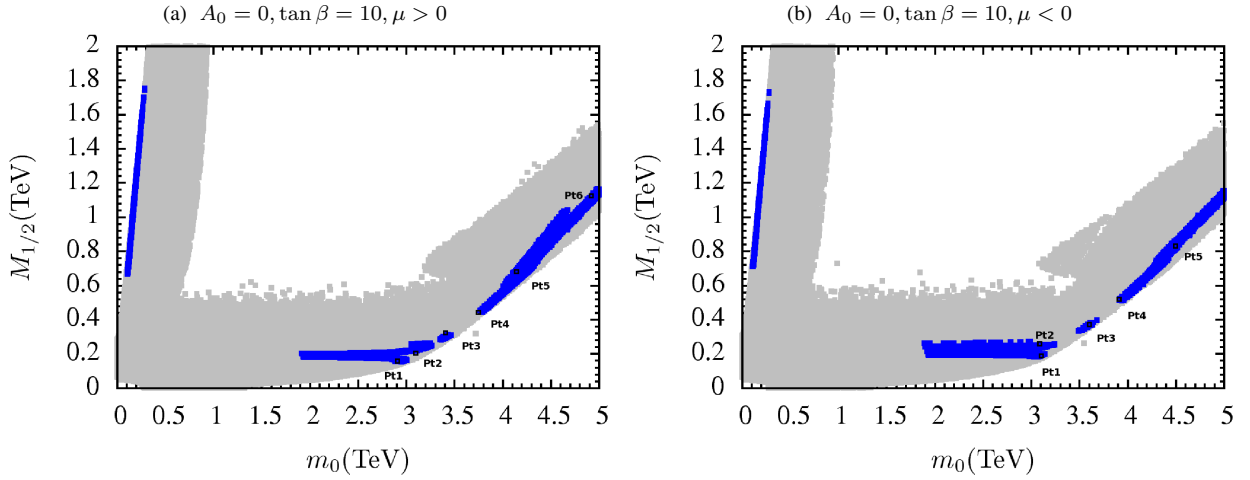


FIG. 1: Plots in the $(M_{1/2}, m_0)$ plane. Gray points are consistent with REWSB and $\tilde{\chi}_1^0$ LSP. Blue points satisfy the WMAP bounds on $\tilde{\chi}_1^0$ dark matter abundance, particle mass bounds, constraints from $BR(B_s \rightarrow \mu^+ \mu^-)$ and $BR(b \rightarrow s \gamma)$ and $BR(B_u \rightarrow \tau \nu_\tau)$. Approximate locations of benchmark points listed in Tables I and II are also shown.

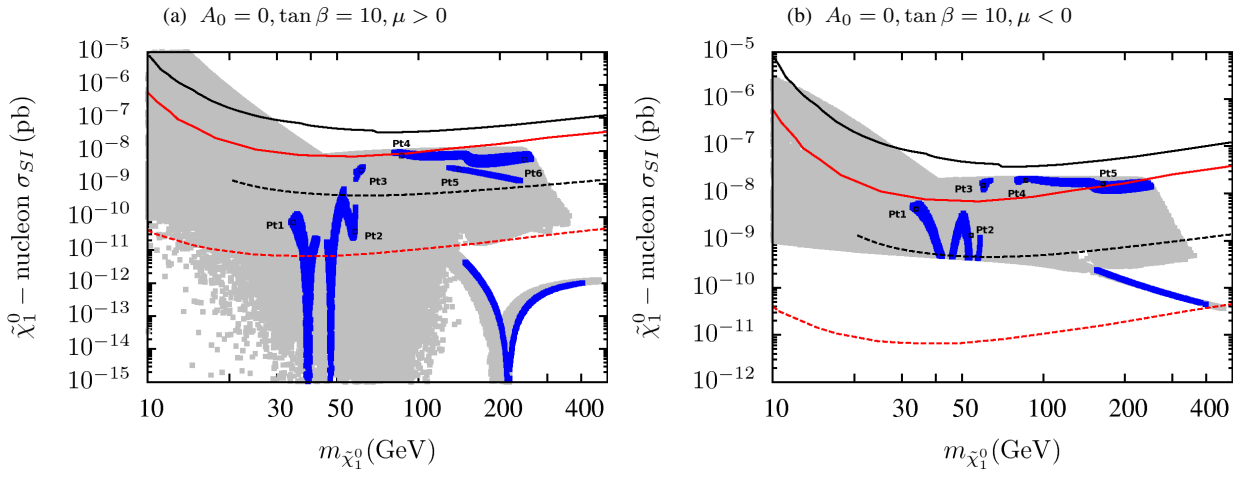


FIG. 2: Spin-independent elastic scattering cross section of neutralino dark matter in the $(\sigma_{SI}, m_{\tilde{\chi}_1^0})$ plane. Color coding is the same as in Figure 1. The current upper bounds from CDMS-II (XENON100) are depicted as black (red) solid lines. Future reach of the SuperCDMS(SNOLAB) (dotted black line) and XENON1T (dotted red line) are shown. Approximate locations of benchmark points listed in Tables I and II are also shown, and which are testable in the ongoing experiments.

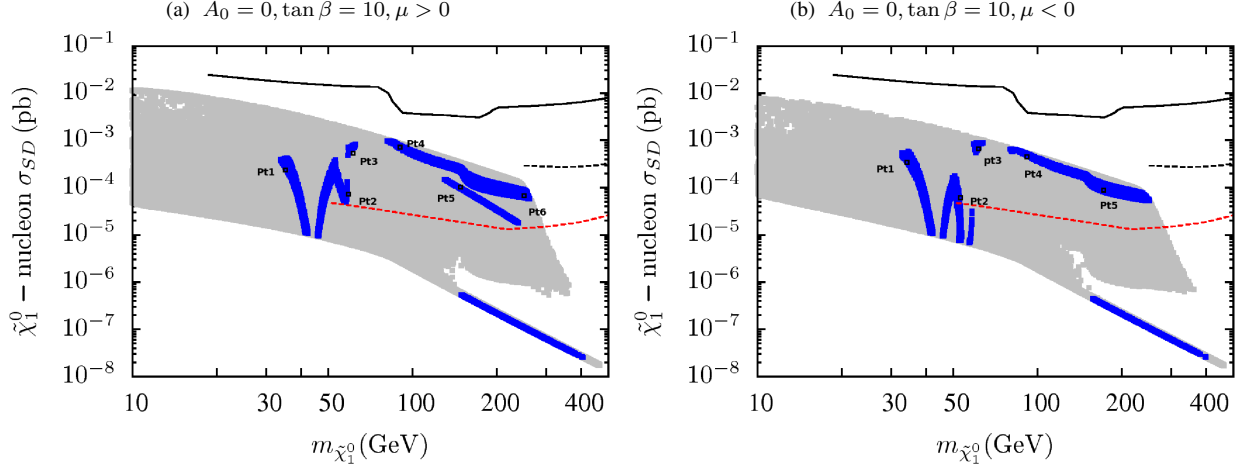


FIG. 3: Spin-dependent elastic scattering cross section of neutralino dark matter in the $(\sigma_{SD}, m_{\tilde{\chi}_1^0})$ plane. Color coding is the same as in Figure 1. Current bounds from Super-Kamiokande (black line), IceCube (dotted black line), and future reach of IceCube DeepCore experiment (dotted red line) are shown. Approximate locations of benchmark points presented in Tables I and II are also shown.

| | Pt1 | Pt2 | Pt3 | Pt4 | Pt5 | Pt6 |
|------------------------------|-----------------------|-----------------------|----------------------|----------------------|----------------------|----------------------|
| m_0 | 2948 | 3134 | 3404 | 3780 | 4384 | 4982 |
| $M_{1/2}$ | 154 | 250 | 292 | 447 | 778 | 1166 |
| A_0 | 0 | 0 | 0 | 0 | 0 | 0 |
| $sign(\mu)$ | + | + | + | + | + | + |
| $\tan \beta$ | 10 | 10 | 10 | 10 | 10 | 10 |
| m_h | 116 | 117 | 118 | 118 | 119 | 119 |
| m_H | 2926 | 3120 | 3387 | 3773 | 4418 | 5078 |
| m_A | 2907 | 3099 | 3365 | 3749 | 4389 | 5045 |
| m_{H^\pm} | 2927 | 3121 | 3388 | 3774 | 4419 | 5079 |
| $m_{\tilde{\chi}_{1,2}^0}$ | 34,108 | 56, 176 | 59,119 | 81, 121 | 170, 234 | 262, 323 |
| $m_{\tilde{\chi}_{3,4}^0}$ | 138,239 | 197, 355 | 127,404 | 132, 603 | 238, 1032 | 330,1537 |
| $m_{\tilde{\chi}_{1,2}^\pm}$ | 104,233 | 168, 345 | 106,391 | 104, 585 | 213, 1006 | 297, 1502 |
| $m_{\tilde{g}}$ | 490 | 733 | 838 | 1207 | 1951 | 2784 |
| $m_{\tilde{u}_{L,R}}$ | 2936,2946 | 3150, 3154 | 3429,3432 | 3863,3855 | 4637, 4596 | 5486,5395 |
| $m_{\tilde{t}_{1,2}}$ | 1687,2402 | 1824, 2587 | 1994,2820 | 2280,3196 | 2819, 3884 | 3433,4657 |
| $m_{\tilde{d}_{L,R}}$ | 2938,2948 | 3151, 3156 | 3430,3434 | 3864,3857 | 4638, 4598 | 5487,5397 |
| $m_{\tilde{b}_{1,2}}$ | 2395,2921 | 2577, 3127 | 2809,3403 | 3184,3822 | 3871, 4556 | 4641,5348 |
| $m_{\tilde{\nu}_1}$ | 2946 | 3137 | 3410 | 3798 | 4441 | 5099 |
| $m_{\tilde{\nu}_3}$ | 2933 | 3124 | 3395 | 3782 | 4423 | 5078 |
| $m_{\tilde{e}_{L,R}}$ | 2946,2945 | 3137, 3131 | 3409,3401 | 3798,3777 | 4440, 4382 | 5097,4982 |
| $m_{\tilde{\tau}_{1,2}}$ | 2919,2933 | 3104, 3123 | 3372,3394 | 3745,3781 | 4345, 4421 | 4940,5076 |
| $\sigma_{SI}(\text{pb})$ | 6.8×10^{-11} | 6.2×10^{-11} | 2.4×10^{-9} | 8.9×10^{-9} | 4.8×10^{-9} | 5.7×10^{-9} |
| $\sigma_{SD}(\text{pb})$ | 3.8×10^{-4} | 8.2×10^{-5} | 7.1×10^{-4} | 9.9×10^{-4} | 1.2×10^{-4} | 6.0×10^{-5} |
| $\Omega_{CDM} h^2$ | 0.13 | 0.1 | 0.10 | 0.12 | 0.1 | 0.13 |

TABLE I: Mass spectra for the benchmark points with $\tan \beta=10$, $\mu > 0$. All of these points satisfy the various constraints mentioned in section III, except $\Delta(g-2)_\mu/2$. Neutralino LSP in all cases has sizeable higgsino component. The points lie between current and future direct and indirect dark matter search limits shown in Figures 2 and 3. Pt1 represents the lightest neutralino and a light gluino. Pts.2 and 3 also have relatively light gluinos.

| | Pt1 | Pt2 | Pt3 | Pt4 | Pt5 |
|------------------------------|----------------------|----------------------|----------------------|----------------------|----------------------|
| m_0 | 3071 | 3061 | 3573 | 3984 | 4490 |
| $M_{1/2}$ | 184 | 249 | 358 | 536 | 855 |
| A_0 | 0 | 0 | 0 | 0 | 0 |
| $sign(\mu)$ | - | - | - | - | - |
| $\tan\beta$ | 10 | 10 | 10 | 10 | 10 |
| m_h | 117 | 117 | 118 | 118 | 119 |
| m_H | 3050 | 3048 | 3560 | 3986 | 4535 |
| m_A | 3030 | 3028 | 3536 | 3960 | 4505 |
| m_{H^\pm} | 3051 | 3049 | 3560 | 3986 | 4536 |
| $m_{\tilde{\chi}_{1,2}^0}$ | 33,110 | 52, 184 | 62, 122 | 98, 147 | 182, 252 |
| $m_{\tilde{\chi}_{3,4}^0}$ | 134, 278 | 209, 362 | 128, 490 | 163, 720 | 262, 1133 |
| $m_{\tilde{\chi}_{1,2}^\pm}$ | 106, 271 | 185, 355 | 112, 478 | 143, 705 | 255, 1113 |
| $m_{\tilde{g}}$ | 567 | 730 | 998 | 1424 | 2119 |
| $m_{\tilde{u}_{L,R}}$ | 3066, 3074 | 3078, 3082 | 3621, 3620 | 4107, 4091 | 4791, 4740 |
| $m_{\tilde{t}_{1,2}}$ | 1765, 2512 | 1783, 2528 | 2119, 2985 | 2443, 3408 | 2932, 4028 |
| $m_{\tilde{d}_{L,R}}$ | 3067, 3076 | 3080, 3084 | 3620, 3622 | 4108, 4093 | 4792, 4742 |
| $m_{\tilde{b}_{1,2}}$ | 2502, 3048 | 2518, 3056 | 2974, 3588 | 3396, 4056 | 4011, 4698 |
| $m_{\tilde{\nu}_1}$ | 3070 | 3065 | 3584 | 4011 | 4558 |
| $m_{\tilde{\nu}_3}$ | 3057 | 3052 | 3568 | 3994 | 4540 |
| $m_{\tilde{e}_{L,R}}$ | 3070, 3068 | 3065, 3058 | 3583, 3570 | 4011, 3981 | 4557, 4488 |
| $m_{\tilde{\tau}_{1,2}}$ | 3041, 3056 | 3017, 3051 | 3539, 3567 | 3947, 3993 | 4450, 4538 |
| $\sigma_{SI}(\text{pb})$ | 5.1×10^{-9} | 1.7×10^{-9} | 1.5×10^{-8} | 1.9×10^{-8} | 1.2×10^{-8} |
| $\sigma_{SD}(\text{pb})$ | 4.8×10^{-4} | 6.5×10^{-5} | 7.1×10^{-4} | 4.1×10^{-4} | 7.9×10^{-5} |
| $\Omega_{CDM}h^2$ | 0.13 | 0.11 | 0.13 | 0.11 | 0.12 |

TABLE II: Mass spectra for the benchmark points for $\tan\beta=10$, $\mu < 0$. All of these points satisfy the various constraints mentioned in section III, except $\Delta(g-2)_\mu/2$. Neutralino LSP in all cases has sizeable higgsino component. The points lie between present and future direct and indirect dark matter search limits shown in Figures 2 and 3. Pt1 represents lightest neutralino, while Pts.1,2,3 have relatively light gluinos.

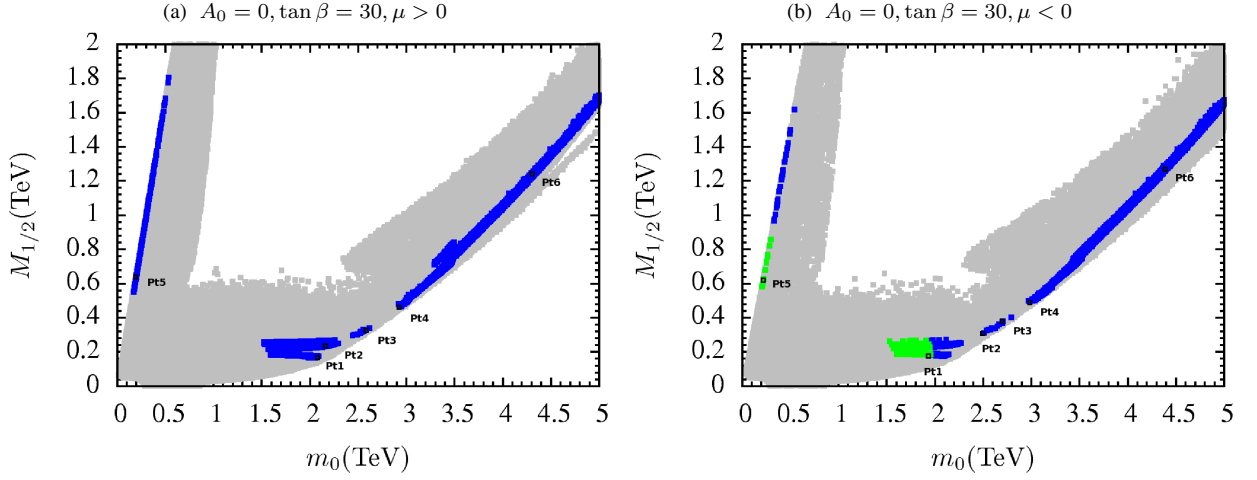


FIG. 4: Plots in the $(M_{1/2}, m_0)$ plane. Gray points are consistent with REWSB and $\tilde{\chi}_1^0$ LSP. Blue points satisfy the WMAP bounds on $\tilde{\chi}_1^0$ dark matter abundance, particle mass bounds, constraints from $BR(B_s \rightarrow \mu^+ \mu^-)$, $BR(b \rightarrow s\gamma)$ and $BR(B_u \rightarrow \tau\nu_\tau)$. Green points belong to the subset of blue points that satisfies all constraints including $\Delta(g-2)_\mu/2$. Approximate locations of benchmark points listed in Tables III and IV are also shown.

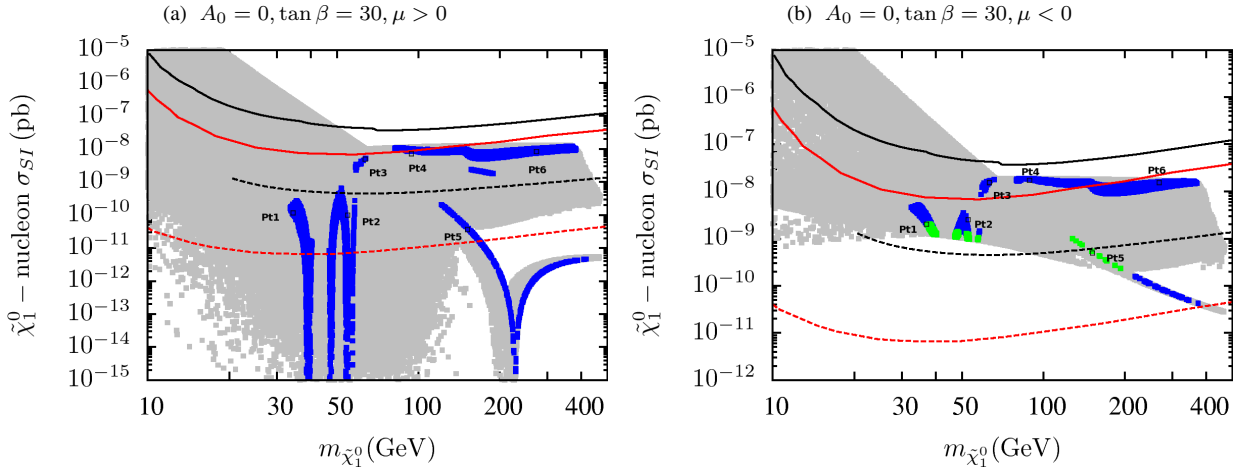


FIG. 5: Spin-independent elastic scattering cross section of neutralino dark matter in the $(\sigma_{SI}, m_{\tilde{\chi}_1^0})$ plane. Color coding is the same as in Figure 4. Current upper bounds from CDMS-II (XENON100) are depicted as solid black (red) lines. Future reach of SuperCDMS(SNOLAB) (dotted black line) and XENON1T (dotted red line) are shown. Approximate locations of benchmark points listed in Tables III and IV are also shown.

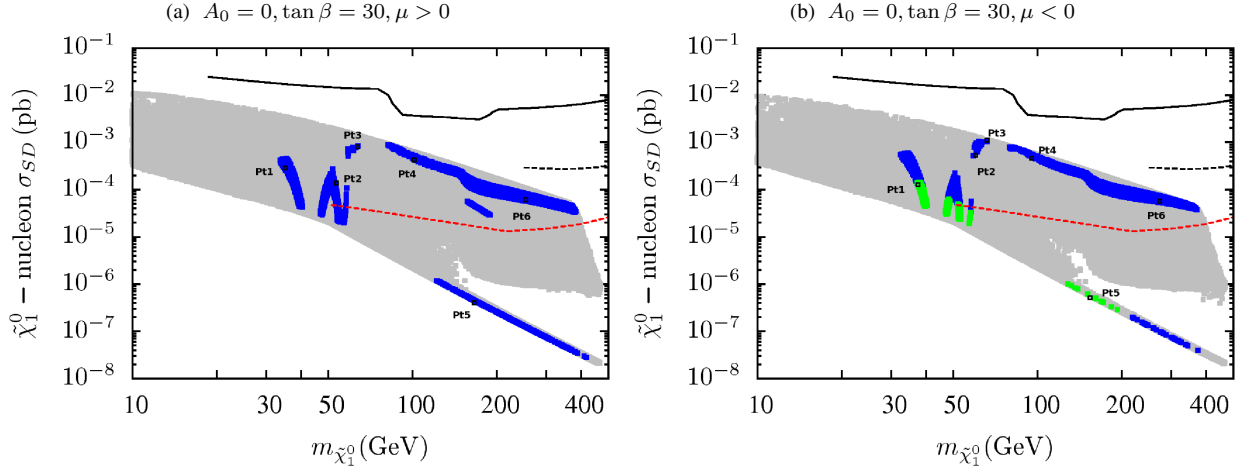


FIG. 6: Spin-dependent elastic scattering cross section of neutralino dark matter in the $(\sigma_{SD}, m_{\tilde{\chi}_1^0})$ plane. Color coding is the same as in Figure 4. Current upper bounds from Super-Kamiokande (black line), IceCube (dotted black line), and future reach of IceCube DeepCore (dotted red line) are shown. Approximate locations of benchmark points listed in Tables III and IV are also shown.

| | Pt1 | Pt2 | Pt3 | Pt4 | Pt5 | Pt6 |
|------------------------------|-----------------------|-----------------------|----------------------|----------------------|-----------------------|----------------------|
| m_0 | 2038 | 2158 | 2616 | 2980 | 201 | 4382 |
| $M_{1/2}$ | 166 | 245 | 341 | 488 | 650 | 1280 |
| A_0 | 0 | 0 | 0 | 0 | 0 | 0 |
| $sign(\mu)$ | + | + | + | + | + | + |
| $\tan \beta$ | 30 | 30 | 30 | 30 | 30 | 30 |
| m_h | 115 | 116 | 117 | 118 | 115 | 120 |
| m_H | 1734 | 1852 | 2247 | 2578 | 800 | 3939 |
| m_A | 1723 | 1840 | 2232 | 2561 | 795 | 3914 |
| m_{H^\pm} | 1737 | 1853 | 2248 | 2579 | 804 | 3940 |
| $m_{\tilde{\chi}_{1,2}^0}$ | 34, 110 | 52, 169 | 64, 123 | 91, 137 | 144, 581 | 283, 337 |
| $m_{\tilde{\chi}_{3,4}^0}$ | 138, 250 | 189, 345 | 124, 463 | 148, 651 | 596, 831 | 349, 1677 |
| $m_{\tilde{\chi}_{1,2}^\pm}$ | 104, 245 | 160, 337 | 103, 450 | 119, 633 | 565, 818 | 311, 1641 |
| $m_{\tilde{g}}$ | 503 | 696 | 934 | 1276 | 1486 | 2990 |
| $m_{\tilde{u}_{L,R}}$ | 2049, 2052 | 2202, 2199 | 2694, 2685 | 3132, 3109 | 1444, 1301 | 5077, 4949 |
| $m_{\tilde{t}_{1,2}}$ | 1184, 1604 | 1289, 1738 | 1595, 2137 | 1888, 2510 | 1068, 1355 | 3264, 4235 |
| $m_{\tilde{d}_{L,R}}$ | 2051, 2053 | 2204, 2201 | 2695, 2686 | 3133, 3110 | 1446, 1300 | 5077, 4950 |
| $m_{\tilde{b}_{1,2}}$ | 1593, 1903 | 1727, 2044 | 2125, 2499 | 2497, 2901 | 1258, 1341 | 4217, 4667 |
| $m_{\tilde{\nu}_1}$ | 2040 | 2166 | 2632 | 3012 | 666 | 4544 |
| $m_{\tilde{\nu}_3}$ | 1960 | 2082 | 2531 | 2898 | 650 | 4381 |
| $m_{\tilde{e}_{L,R}}$ | 2041, 2036 | 2167, 2157 | 2632, 2614 | 3012, 2978 | 673, 233 | 4544, 4384 |
| $m_{\tilde{\tau}_{1,2}}$ | 1874, 1960 | 1985, 2083 | 2408, 2531 | 2744, 2898 | 152, 659 | 4038, 4379 |
| $\sigma_{SI}(\text{pb})$ | 1.6×10^{-10} | 1.5×10^{-10} | 5.2×10^{-9} | 9.5×10^{-9} | 6.0×10^{-11} | 8.9×10^{-9} |
| $\sigma_{SD}(\text{pb})$ | 4.2×10^{-4} | 1.0×10^{-4} | 8.4×10^{-3} | 6.5×10^{-4} | 7.0×10^{-7} | 5.9×10^{-5} |
| $\Omega_{CDM} h^2$ | 0.13 | 0.11 | 0.13 | 0.1 | 0.1 | 0.1 |

TABLE III: Mass spectra for the benchmark points for $\tan \beta=30$, $\mu > 0$. All of these points satisfy the various constraints mentioned in section III, except $\Delta(g-2)_\mu/2$. For all points, the neutralino LSP has sizeable higgsino component. The points lie between present and future direct and indirect dark matter search limits shown in Figures 5 and 6. Pt1 represents lightest neutralino scenario and Pt5 shows stau-coannihilation scenario.

| | Pt1 | Pt2 | Pt3 | Pt4 | Pt5 | Pt6 |
|------------------------------|----------------------|----------------------|----------------------|----------------------|-----------------------|----------------------|
| m_0 | 1939 | 2510 | 2790 | 3070 | 219 | 4490 |
| $M_{1/2}$ | 183 | 311 | 402 | 525 | 616 | 1340 |
| A_0 | 0 | 0 | 0 | 0 | 0 | 0 |
| $sign(\mu)$ | - | - | - | - | - | - |
| $\tan\beta$ | 30 | 30 | 30 | 30 | 30 | 30 |
| m_h | 115 | 117 | 118 | 119 | 115 | 121 |
| m_H | 1640 | 2139 | 2390 | 2650 | 695 | 400 |
| m_A | 1629 | 2125 | 2374 | 2630 | 690 | 3970 |
| m_{H^\pm} | 1642 | 2141 | 2391 | 2650 | 700 | 4000 |
| $m_{\tilde{\chi}_{1,2}^0}$ | 37,142 | 59,130 | 66,112 | 96,142 | 136,553 | 290,337 |
| $m_{\tilde{\chi}_{3,4}^0}$ | 177,279 | 135,425 | 126,541 | 157,700 | 569,791 | 355,1750 |
| $m_{\tilde{\chi}_{1,2}^\pm}$ | 142,276 | 123,417 | 104,530 | 138,686 | 559,784 | 344,1720 |
| $m_{\tilde{g}}$ | 542 | 861 | 1078 | 1360 | 1420 | 3100 |
| $m_{\tilde{u}_{L,R}}$ | 1960,1961 | 2576,2568 | 2896,2881 | 3240,3200 | 1380,1240 | 5200,5090 |
| $m_{\tilde{t}_{1,2}}$ | 1137,1534 | 1519,2035 | 1728,2303 | 1960,2600 | 1020,1280 | 3370,4350 |
| $m_{\tilde{d}_{L,R}}$ | 1962,1963 | 2577,2570 | 2897,2884 | 3240,3220 | 1380,1240 | 5230,5090 |
| $m_{\tilde{b}_{1,2}}$ | 1524,1810 | 2023,2382 | 2291,2679 | 2590,2990 | 1170,1270 | 4330,4780 |
| $m_{\tilde{\nu}_1}$ | 1942 | 2523 | 2812 | 3110 | 641 | 4660 |
| $m_{\tilde{\nu}_3}$ | 1865 | 2425 | 2704 | 2990 | 622 | 4490 |
| $m_{\tilde{e}_{L,R}}$ | 1944,1938 | 2523,2508 | 2812,2788 | 3110,3070 | 648,247 | 4660,4490 |
| $m_{\tilde{\tau}_{1,2}}$ | 1779,1866 | 2307,2425 | 2566,2703 | 2820,2990 | 145,633 | 4130,4490 |
| $\sigma_{SI}(\text{pb})$ | 1.9×10^{-9} | 8.6×10^{-9} | 1.8×10^{-8} | 1.7×10^{-8} | 7.9×10^{-10} | 1.5×10^{-8} |
| $\sigma_{SD}(\text{pb})$ | 1.4×10^{-4} | 5.3×10^{-4} | 1.0×10^{-3} | 5.3×10^{-4} | 8.4×10^{-7} | 6.0×10^{-5} |
| $\Omega_{CDM}h^2$ | 0.13 | 0.12 | 0.13 | 0.1 | 0.13 | 0.1 |

TABLE IV: Mass spectra for the benchmark points for $\tan\beta=30$, $\mu < 0$. All of these points satisfy the various constraints mentioned in section III. For all points, the neutralino LSP has sizeable higgsino component. The points lie between present and future direct and indirect dark matter search limits shown in Figures 5 and 6. Pt1 shows the lightest neutralino and also a light gluino. Pt5 shows a stau-coannihilation scenario.

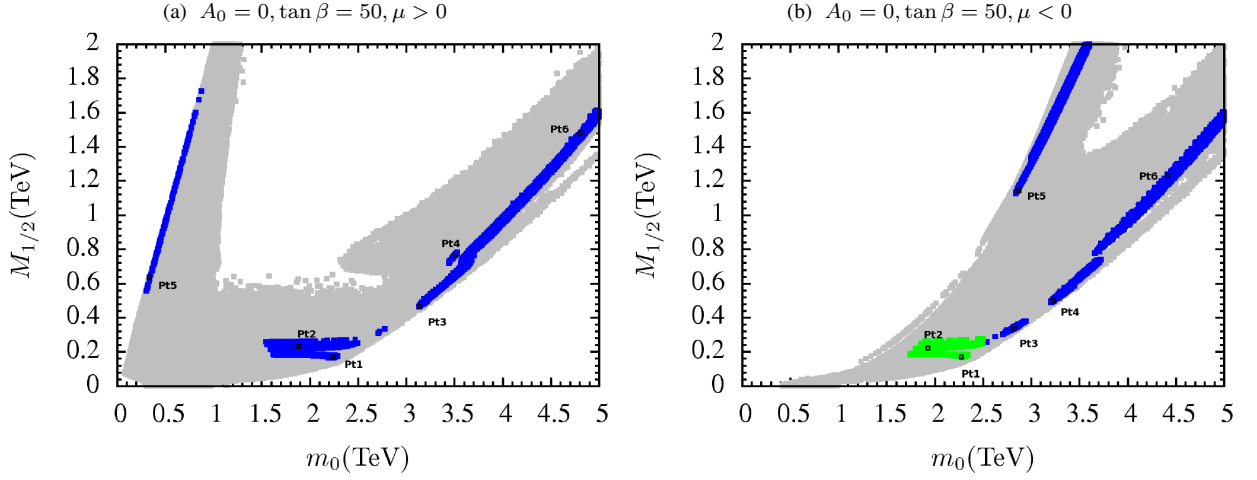


FIG. 7: Plots in the $(M_{1/2}, m_0)$ plane. Gray points are consistent with REWSB and $\tilde{\chi}_1^0$ LSP. Blue points satisfy the WMAP bounds on $\tilde{\chi}_1^0$ dark matter abundance, particle mass bounds, constraints from $BR(B_s \rightarrow \mu^+ \mu^-)$, $BR(b \rightarrow s \gamma)$ and $BR(B_u \rightarrow \tau \nu_\tau)$. Green points belong to the subset of blue points that satisfies all constraints including $\Delta(g-2)_\mu/2$. Approximate locations of benchmark points listed in Tables V and VI are also shown.

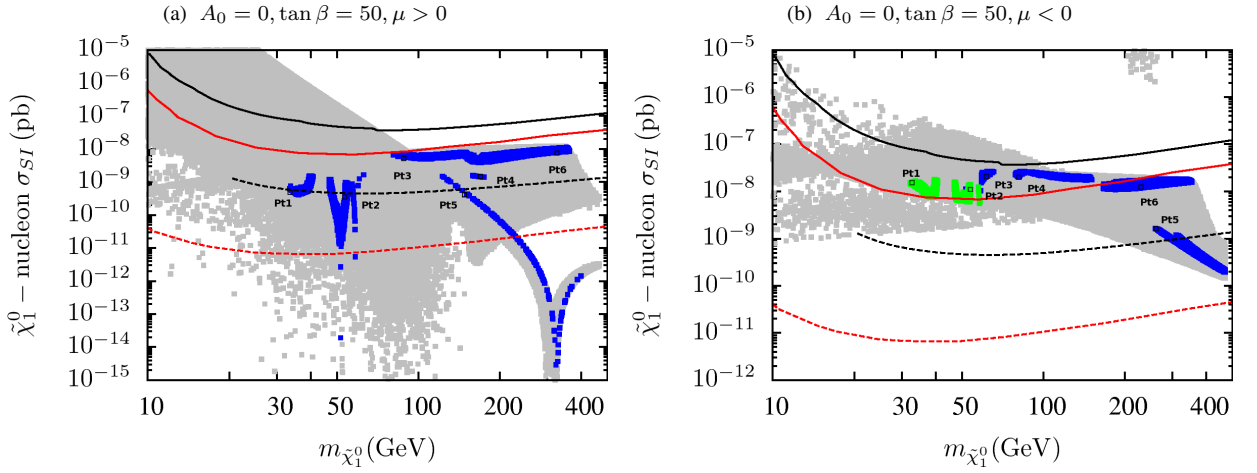


FIG. 8: Spin-independent elastic scattering cross section of neutralino dark matter in the $(\sigma_{SI}, m_{\tilde{\chi}_1^0})$ plane. Color coding is same as in Figure 4. Current upper bounds from the CDMS-II (XENON100) are depicted as solid black (red) lines. Future reach of SuperCDMS(SNOLAB) (dotted black line) and XENON1T (dotted red line) are shown. Approximate locations of benchmark points listed in Tables V and VI are also shown.

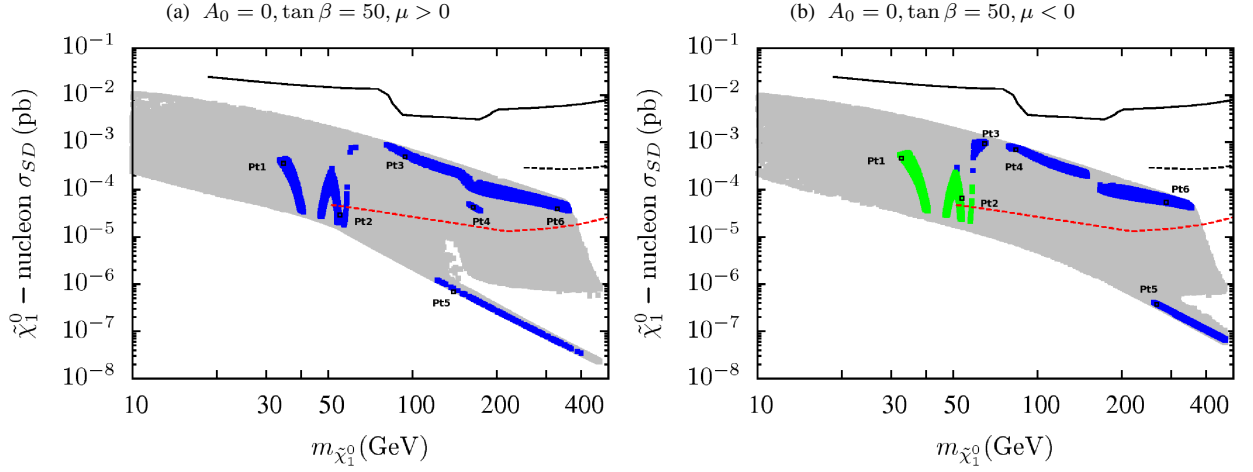


FIG. 9: Spin-dependent elastic scattering cross section versus neutralino dark matter mass. Color coding is the same as in Figure 4. Current bounds from Super-Kamiokande (black line) and IceCube (dotted black line), and future reach of IceCube DeepCore (dotted red line) are shown. Approximate locations of benchmark points listed in Tables V and VI are also shown.

| | Pt1 | Pt2 | Pt3 | Pt4 | Pt5 | Pt6 |
|------------------------------|-----------------------|-----------------------|----------------------|----------------------|-----------------------|----------------------|
| m_0 | 2241 | 1851 | 3175 | 3529 | 392 | 4765 |
| $M_{1/2}$ | 167 | 247 | 489 | 783 | 735 | 1440 |
| A_0 | 0 | 0 | 0 | 0 | 0 | 0 |
| $sign(\mu)$ | + | + | + | + | + | + |
| $\tan \beta$ | 50 | 50 | 50 | 50 | 50 | 50 |
| m_h | 116 | 115 | 119 | 120 | 116 | 121 |
| m_H | 1046 | 967 | 1609 | 1944 | 750 | 2802 |
| m_A | 1039 | 961 | 1598 | 1932 | 745 | 2785 |
| m_{H^\pm} | 1050 | 972 | 1613 | 1947 | 755 | 2803 |
| $m_{\tilde{\chi}_{1,2}^0}$ | 33, 111 | 54, 225 | 90, 136 | 175, 287 | 165, 642 | 320, 371 |
| $m_{\tilde{\chi}_{3,4}^0}$ | 138, 252 | 257, 357 | 148, 654 | 287, 1032 | 655, 938 | 386, 1886 |
| $m_{\tilde{\chi}_{1,2}^\pm}$ | 104, 247 | 218, 350 | 119, 636 | 264, 1007 | 623, 923 | 344, 1845 |
| $m_{\tilde{g}}$ | 509 | 693 | 1284 | 1928 | 1669 | 3326 |
| $m_{\tilde{u}_{L,R}}$ | 2249, 2253 | 1913, 1906 | 3317, 3296 | 3868, 3808 | 1649, 1490 | 5564, 5416 |
| $m_{\tilde{t}_{1,2}}$ | 1300, 1578 | 1130, 1387 | 1993, 2423 | 2407, 2934 | 1210, 1508 | 3593, 4386 |
| $m_{\tilde{d}_{L,R}}$ | 2251, 2255 | 1914, 1907 | 3318, 3298 | 3868, 3809 | 1651, 1489 | 5565, 5417 |
| $m_{\tilde{b}_{1,2}}$ | 1564, 1777 | 1373, 1545 | 2407, 2672 | 2917, 3170 | 1375, 1496 | 4362, 4614 |
| $m_{\tilde{\nu}_1}$ | 2242 | 1862 | 3205 | 3604 | 817 | 4954 |
| $m_{\tilde{\nu}_3}$ | 1984 | 1654 | 2850 | 3217 | 770 | 4444 |
| $m_{\tilde{e}_{L,R}}$ | 2243, 2239 | 1864, 1850 | 3206, 3173 | 3604, 3528 | 823, 414 | 4953, 4768 |
| $m_{\tilde{\tau}_{1,2}}$ | 1683, 1984 | 1397, 1654 | 2400, 2859 | 2677, 3215 | 173, 779 | 3621, 4440 |
| $\sigma_{SI}(\text{pb})$ | 6.3×10^{-10} | 4.5×10^{-10} | 6.2×10^{-9} | 1.4×10^{-9} | 2.5×10^{-10} | 8.9×10^{-9} |
| $\sigma_{SD}(\text{pb})$ | 4.2×10^{-4} | 2.7×10^{-5} | 6.5×10^{-4} | 3.6×10^{-5} | 4.9×10^{-7} | 4.9×10^{-5} |
| $\Omega_{CDM} h^2$ | 0.13 | 0.11 | 0.1 | 0.13 | 0.13 | 0.1 |

TABLE V: Benchmark points for $\tan \beta=50$, $\mu > 0$. All of these points satisfy the various constraints mentioned in section III, except $\Delta(g-2)_\mu/2$. In all cases, the neutralino LSP has sizeable higgsino component. The points lie between present and future direct and indirect searches of dark matter shown in Figures 8 and 9. Pt1 represents lightest neutralino, and Pt5 shows stau-coannihilation scenario. Pts.1, and 2 show relatively light gluinos.

| | Pt1 | Pt2 | Pt3 | Pt4 | Pt5 | Pt6 |
|------------------------------|----------------------|----------------------|----------------------|----------------------|----------------------|----------------------|
| m_0 | 2237 | 1944 | 2893 | 3248 | 2856 | 4495 |
| $M_{1/2}$ | 174 | 246 | 368 | 509 | 1148 | 1259 |
| A_0 | 0 | 0 | 0 | 0 | 0 | 0 |
| $sign(\mu)$ | - | - | - | - | - | - |
| $\tan\beta$ | 50 | 50 | 50 | 50 | 50 | 50 |
| m_h | 116 | 115 | 118 | 119 | 119 | 121 |
| m_H | 902 | 618 | 1276 | 1486 | 593 | 2200 |
| m_A | 896 | 614 | 1267 | 1476 | 589 | 2185 |
| m_{H^\pm} | 907 | 624 | 1279 | 1489 | 600 | 2202 |
| $m_{\tilde{\chi}_{1,2}^0}$ | 34, 115 | 53, 217 | 64, 117 | 84, 121 | 265, 745 | 276, 330 |
| $m_{\tilde{\chi}_{3,4}^0}$ | 143, 264 | 251, 358 | 124, 498 | 145, 679 | 749, 1487 | 344, 1650 |
| $m_{\tilde{\chi}_{1,2}^\pm}$ | 114, 259 | 219, 355 | 108, 487 | 116, 666 | 760, 1465 | 336, 1625 |
| $m_{\tilde{g}}$ | 527 | 693 | 1001 | 1330 | 2643 | 2949 |
| $m_{\tilde{u}_{L,R}}$ | 2248, 2251 | 2001, 1995 | 2975, 2965 | 3399, 3376 | 3711, 3562 | 5154, 5033 |
| $m_{\tilde{t}_{1,2}}$ | 1302, 1554 | 1181, 1381 | 1764, 2115 | 2047, 2457 | 2469, 2880 | 3300, 3957 |
| $m_{\tilde{d}_{L,R}}$ | 2250, 2253 | 2003, 1996 | 2976, 2967 | 3398, 3378 | 3712, 3561 | 5154, 5034 |
| $m_{\tilde{b}_{1,2}}$ | 1539, 1730 | 1366, 1495 | 2099, 2333 | 2440, 2686 | 2791, 2861 | 3935, 4137 |
| $m_{\tilde{\nu}_1}$ | 2239 | 1955 | 2910 | 3281 | 3059 | 4648 |
| $m_{\tilde{\nu}_3}$ | 1973 | 1717 | 2575 | 2906 | 2704 | 4135 |
| $m_{\tilde{e}_{L,R}}$ | 2240, 2235 | 1956, 1942 | 2911, 2891 | 3281, 3246 | 3060, 2861 | 4648, 4496 |
| $m_{\tilde{\tau}_{1,2}}$ | 1662, 1974 | 1424, 1718 | 2163, 2574 | 2432, 2906 | 2017, 2701 | 3341, 4131 |
| $\sigma_{SI}(\text{pb})$ | 1.3×10^{-8} | 1.0×10^{-8} | 2.6×10^{-8} | 2.6×10^{-8} | 1.5×10^{-9} | 1.4×10^{-8} |
| $\sigma_{SD}(\text{pb})$ | 3.7×10^{-4} | 3.0×10^{-5} | 7.8×10^{-4} | 7.8×10^{-4} | 3.8×10^{-7} | 5.9×10^{-5} |
| $\Omega_{CDM}h^2$ | 0.13 | 0.11 | 0.12 | 0.11 | 0.11 | 0.12 |

TABLE VI: Benchmark points for $\tan\beta=50$, $\mu < 0$. All of these points satisfy the various constraints mentioned in section III. For all points, the neutralino LSP has sizeable higgsino component. The points lie between present and future direct and indirect dark matter search limits shown in Figures 8 and 9. Pt1 shows lightest neutralino and a light gluino. Pt5 shows stau-coannihilation.

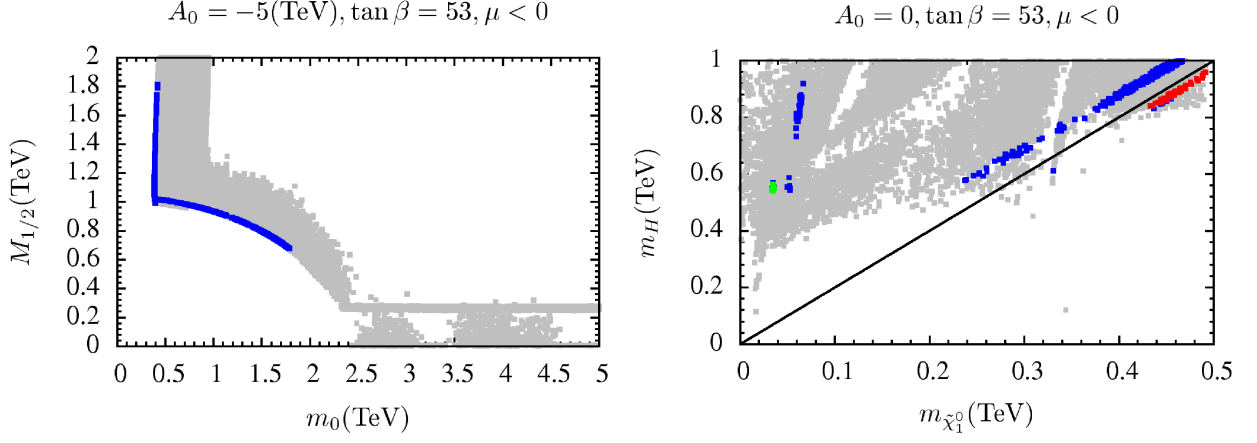


FIG. 10: Plots in the $(M_{1/2}, m_0)$ and $(m_H, m_{\tilde{\chi}_1^0})$ planes. Gray points are consistent with REWSB and $\tilde{\chi}_1^0$ LSP. Blue points satisfy the WMAP bounds on $\tilde{\chi}_1^0$ dark matter abundance, particle mass bounds, constraints from $BR(B_s \rightarrow \mu^+ \mu^-)$, $BR(b \rightarrow s\gamma)$ and $BR(B_u \rightarrow \tau \nu_\tau)$. Green points belong to the subset of blue points that satisfies all constraints including $\Delta(g-2)_\mu/2$. Red points satisfy criterion of $|2m_{\tilde{\chi}_1^0} - m_H| \leq 30$.

| | Pt1 | Pt2 | Pt3 |
|------------------------------|-----------------------|-----------------------|-----------------------|
| m_0 | 1771 | 1751 | 4892 |
| $M_{1/2}$ | 686 | 696 | 2075 |
| A_0 | -5000 | -5000 | 0 |
| $sign(\mu)$ | - | - | - |
| $\tan \beta$ | 10 | 10 | 53 |
| m_h | 123 | 122 | 122 |
| m_H | 2657 | 2650 | 947 |
| m_A | 2640 | 2633 | 940 |
| m_{H^\pm} | 2658 | 2652 | 951 |
| $m_{\tilde{\chi}_{1,2}^0}$ | 154, 879 | 156, 892 | 488, 879 |
| $m_{\tilde{\chi}_{3,4}^0}$ | 1929, 1932 | 1934, 1938 | 880, 2696 |
| $m_{\tilde{\chi}_{1,2}^\pm}$ | 886, 1938 | 899, 1944 | 900, 2658 |
| $m_{\tilde{g}}$ | 1648 | 1669 | 4578 |
| $m_{\tilde{u}_{L,R}}$ | 2303, 2217 | 2303, 2214 | 6398, 6119 |
| $m_{\tilde{t}_{1,2}}$ | 188, 1695 | 196, 1697 | 4289, 5030 |
| $m_{\tilde{d}_{L,R}}$ | 2305, 2218 | 2304, 2215 | 6398, 6119 |
| $m_{\tilde{b}_{1,2}}$ | 1700, 2144 | 1703, 2141 | 4876, 5001 |
| $m_{\tilde{\nu}_1}$ | 1889 | 1873 | 5270 |
| $m_{\tilde{\nu}_3}$ | 1865 | 1849 | 4597 |
| $m_{\tilde{e}_{L,R}}$ | 1887, 1775 | 1872, 1755 | 5270, 4901 |
| $m_{\tilde{\tau}_{1,2}}$ | 1717, 1864 | 1697, 1849 | 3270, 4592 |
| $\sigma_{SI}(\text{pb})$ | 1.2×10^{-11} | 1.2×10^{-11} | 7.8×10^{-10} |
| $\sigma_{SD}(\text{pb})$ | 1.4×10^{-9} | 2.3×10^{-9} | 5.2×10^{-7} |
| $\Omega_{CDM} h^2$ | 0.12 | 0.13 | 0.1 |

TABLE VII: Pts.1 and 2 correspond to stop-neutralino coannihilation region, while Pt3 belongs in the so-called H-funnel region.

| | NUGM | CMSSM | NUGM | CMSSM | NUGM | CMSSM | NUGM | CMSSM |
|------------------------------|-----------------------|-----------------------|-----------------------|-----------------------|-----------------------|-----------------------|-----------------------|----------------------|
| m_0 | 287 | 199 | 538 | 268 | 219 | 150 | 440 | 276 |
| $M_{1/2}$ | 1687 | 918 | 1188 | 650 | 1258 | 691 | 1040 | 572 |
| A_0 | 1000 | 1000 | 1000 | 1000 | 1000 | 1000 | 1000 | 1000 |
| $sign(\mu)$ | - | - | - | - | + | + | + | + |
| $\tan\beta$ | 10 | 10 | 30 | 30 | 10 | 10 | 30 | 30 |
| m_h | 118 | 116 | 118 | 115 | 117 | 115 | 117 | 115 |
| m_H | 2071 | 1160 | 1289 | 726 | 1587 | 888 | 1233 | 687 |
| m_A | 2057 | 1152 | 1281 | 721 | 1576 | 882 | 1225 | 683 |
| m_{H^\pm} | 2073 | 1163 | 1292 | 731 | 1589 | 892 | 1236 | 692 |
| $m_{\tilde{\chi}_{1,2}^0}$ | 388, 1277 | 388, 732 | 271, 933 | 271, 509 | 287, 1005 | 287, 538 | 236, 840 | 236, 442 |
| $m_{\tilde{\chi}_{3,4}^0}$ | 1281, 2146 | 976, 984 | 940, 1512 | 704, 716 | 1011, 1597 | 750, 767 | 847, 1322 | 628, 644 |
| $m_{\tilde{\chi}_{1,2}^\pm}$ | 1298, 2121 | 733, 983 | 948, 1496 | 509, 715 | 971, 1574 | 539, 767 | 811, 1302 | 443, 645 |
| $m_{\tilde{g}}$ | 3594 | 2020 | 2601 | 1470 | 2736 | 1553 | 2298 | 1307 |
| $m_{\tilde{u}_{L,R}}$ | 3474, 3084 | 1848, 1776 | 2557, 2293 | 1364, 1315 | 2645, 2357 | 1423, 1369 | 2252, 2021 | 1220, 1178 |
| $m_{\tilde{t}_{1,2}}$ | 2547, 3285 | 1490, 1751 | 1875, 2363 | 1095, 1273 | 2502, 1235 | 1145, 1358 | 1655, 2102 | 975, 1148 |
| $m_{\tilde{d}_{L,R}}$ | 3475, 3080 | 1850, 1769 | 2558, 2290 | 1366, 1310 | 2646, 2354 | 1425, 1364 | 2253, 2019 | 1223, 1174 |
| $m_{\tilde{b}_{1,2}}$ | 3065, 3268 | 1727, 1760 | 2180, 2348 | 1230, 1270 | 2344, 2487 | 1330, 1359 | 1960, 2086 | 1108, 1151 |
| $m_{\tilde{\nu}_1}$ | 1644 | 636 | 1269 | 505 | 1234 | 479 | 1101 | 466 |
| $m_{\tilde{\nu}_3}$ | 1627 | 628 | 1211 | 478 | 1221 | 472 | 1056 | 433 |
| $m_{\tilde{e}_{L,R}}$ | 1651, 398 | 645, 393 | 1275, 576 | 513, 362 | 1242, 301 | 489, 298 | 1107, 476 | 475, 350 |
| $m_{\tilde{\tau}_{1,2}}$ | 388, 1640 | 388, 640 | 276, 1220 | 276, 496 | 290, 286 | 290, 484 | 241, 1064 | 241, 450 |
| $\sigma_{SI}(\text{pb})$ | 5.4×10^{-11} | 5.0×10^{-12} | 9.9×10^{-11} | 3.7×10^{-11} | 7.5×10^{-13} | 3.6×10^{-10} | 3.0×10^{-10} | 1.1×10^{-9} |
| $\sigma_{SD}(\text{pb})$ | 3.4×10^{-8} | 1.0×10^{-7} | 1.2×10^{-7} | 4.2×10^{-7} | 8.5×10^{-8} | 3.1×10^{-7} | 7.1×10^{-7} | 7.0×10^{-7} |
| $\Omega_{CDM}h^2$ | 0.13 | 0.13 | 0.12 | 0.08 | 0.12 | 0.12 | 0.11 | 0.08 |

TABLE VIII: Particle masses for NUGM and CMSSM benchmark points in the stau-neutralino coannihilation region. The parameters m_0 and $M_{1/2}$ in the CMSSM are tuned so as to yield the same neutralino LSP and $\tilde{\tau}$ masses as in the NUGM for each benchmark point. We observe that masses of remaining particles can differ widely. Results for $\Omega_{CDM}h^2$ in CMSSM are within 5- σ range of the WMAP constraints.

| | NUGM | CMSSM | NUGM | CMSSM | NUGM | CMSSM | NUGM | CMSSM |
|------------------------------|-----------|-----------|-----------|-----------|-----------|-----------|-----------|-----------|
| m_0 | 541 | 423 | 1690 | 1690 | 1700 | 1699 | 1684 | 1683 |
| $M_{1/2}$ | 1203 | 1218 | 201 | 203 | 187 | 188 | 217 | 219 |
| A_0 | 1000 | 1000 | -1000 | -1000 | 0 | 0 | 0 | 0 |
| $sign(\mu)$ | - | - | + | + | - | - | + | + |
| $\tan\beta$ | 30 | 30 | 30 | 30 | 30 | 30 | 50 | 50 |
| m_h | 118 | 119 | 115 | 115 | 114.4 | 115 | 114.4 | 114.5 |
| m_H | 1303 | 1318 | 1472 | 1461 | 1439 | 1444 | 875 | 781 |
| m_A | 1294 | 1310 | 1463 | 1451 | 1429 | 1434 | 869 | 775 |
| m_{H^\pm} | 1305 | 1321 | 1475 | 1463 | 1441 | 1446 | 880 | 786 |
| $m_{\tilde{\chi}_{1,2}^0}$ | 275,940 | 523,980 | 44,248 | 85,165 | 39,172 | 77,141 | 47,208 | 89,162 |
| $m_{\tilde{\chi}_{3,4}^0}$ | 947,1531 | 1243,1252 | 408,421 | 472,480 | 219,295 | 254,271 | 247,325 | 289,312 |
| $m_{\tilde{\chi}_{1,2}^\pm}$ | 956,1514 | 981,1252 | 247,423 | 166,482 | 172,294 | 139,272 | 202,320 | 163,311 |
| $m_{\tilde{g}}$ | 2631 | 2631 | 583 | 583 | 546 | 546 | 617 | 617 |
| $m_{\tilde{u}_{L,R}}$ | 2582,2318 | 2423,2328 | 1731,1728 | 1725,1729 | 1732,1730 | 1726,1730 | 1736,1730 | 1727,1730 |
| $m_{\tilde{t}_{1,2}}$ | 1896,2390 | 1939,2242 | 977,1349 | 964,1331 | 1010,1357 | 1012,1353 | 1023,1256 | 1025,1232 |
| $m_{\tilde{d}_{L,R}}$ | 2587,2315 | 2423,2315 | 1733,1729 | 1726,1729 | 1734,1731 | 1727,1731 | 1737,1731 | 1730,1731 |
| $m_{\tilde{b}_{1,2}}$ | 2205,2376 | 2202,2236 | 1337,1594 | 1318,1583 | 1346,1540 | 1341,1597 | 1241,1399 | 1215,1373 |
| $m_{\tilde{\nu}_1}$ | 1283 | 905 | 1697 | 1691 | 1705 | 1699 | 1693 | 1685 |
| $m_{\tilde{\nu}_3}$ | 1226 | 876 | 1625 | 1614 | 1636 | 1631 | 1502 | 1480 |
| $m_{\tilde{e}_{L,R}}$ | 1289,580 | 912,616 | 1698,1690 | 1692,1690 | 1707,1699 | 1700,1699 | 1695,1683 | 1686,1683 |
| $m_{\tilde{\tau}_{1,2}}$ | 278,1233 | 541,890 | 1542,1627 | 1532,1616 | 1558,1638 | 1562,1633 | 1269,1504 | 1240,1482 |

TABLE IX: Comparison of particle masses of NUGM and CMSSM benchmark points with m_0 and $M_{1/2}$ in CMSSM tuned to give the same $m_{\tilde{g}}$ and $m_{\tilde{d}_R}$ as in NUGM.